Chinese Chemical Letters 33 (2022) 1831–1840

Contents lists available at ScienceDirect

Chinese Chemical Letters

journal homepage: www.elsevier.com/locate/cclet

Emerging two-dimensional nanocatalysts for electrocatalytic hydrogen production

Hong Chen, Yansong Zhou, Wei Guo*, Bao Yu Xia*

Key Laboratory of Material Chemistry for Energy Conversion and Storage (Ministry of Education), Hubei Key Laboratory of Material Chemistry and Service Failure, Hubei Engineering Research Center for Biomaterials and Medical Protective Materials, Wuhan National Laboratory for Optoelectronics, School of Chemistry and Chemical Engineering, Huazhong University of Science and Technology (HUST), Wuhan 430074, China

ARTICLE INFO

Article history:
Received 25 June 2021
Revised 24 July 2021
Accepted 8 September 2021
Available online 13 September 2021

Keywords:
Hydrogen evolution
Electrocatalyst
Two-dimensional
Active sites
Modification

ABSTRACT

Hydrogen energy could be a economic and powerful technology for sustainable future. Producing hydrogen fuel by electrochemical water splitting has attracted intense interest. Due to their physical and chemical properties, two-dimensional (2D) nanomaterials have sparked immense interest in water electrocatalysis for hydrogen production. This review focuses on the emerging nanocatalysts in 2D nanoarchitectures for electrocatalytic hydrogen production. The fundamentals of HER are firstly depicted, following the discussion of recent advances in typical 2D electrocatalysts for HER. The insights into the relationship among the synthetic protocols, structure, catalytic performance and thermodynamics will be discussed in details. Finally, the outlooks regarding further development of 2D nanocatalysts for HER are proposed. We hope this review will offer a comprehensive understanding in 2D nanocatalysts to promote electrochemical hydrogen production.

1. Introduction

In recent years, the exponentially increased population and rapidly developed industrialization have raised the energy demand of human society [1]. Due to the exhaustion and environmental pollution of traditional fossil fuels, the exploration of alternative green energy carriers has drawn massive attention [2]. Hydrogen is considered as a promising clean energy carrier owing to its renewability and remarkable gravimetric energy density (140 MJ/kg) [3,4]. Generally, hydrogen can be produced by photocatalytic and electrochemical water splitting, steam reforming process, iodine-sulfur cycle, and so on [5,6]. Compared to other technologies, electrocatalytic water splitting driven by sustainable energy would be more promising [7,8].

Like many chemical reactions, the electrochemical hydrogen evolution reaction (HER) requires high energy input called overpotential to overcome the barrier. Suitable catalysts are necessary to minimize the overpotential for HER. Generally, homogeneous catalysts have identified active sites with high catalytic activity and selectivity, but they usually have drawbacks of undesirable durability and post-reaction separation [9]. By contrast, heterogeneous catalysts have several advantages over homogeneous ones, and they are considered as potential candidates [10]. Among them, metal-based catalysts, especially noble metals such as platinum, has a minimized free energy for hydrogen absorption and reduced overpotential for hydrogen production. However, the rarity and expensive nature of noble metals limit their practical application in large-scale water electrocatalysis. Thereby, various earth-abundant catalysts have been considered in different nanostructured architectures, including nanoparticles, nanowires, nanosheets, nanotubes, nanobelts, superlattices, *etc*. [11,12]. Particularly, nanomaterials in two-dimension (2D) have emerged as a hotspot for nanocatalysts due to their unique structure as well as remarkable physical and electronic properties [13].

In the past few years, 2D materials play an increasingly important role in efficient water electrolysis for hydrogen production, it is necessary to comprehensively summarize their research progress of 2D nanocatalysts for hydrogen evolution. In this feature review, we first introduce the fundamentals and performance evaluation criteria of HER. Then, the advances of 2D electrocatalysts in electrochemical HER will be discussed in details. The 2D electrocatalysts are classified into organic composites, such as metal organic frameworks (MOFs) [14,15], covalent organic frameworks (COFs) [16]; and inorganic nanocatalysts, including metallic nanomaterials [17], metal-free nanomaterials [18,19], transition metal dichalcogenides (TMDs) [20,21], MXenes [22] and layered double hydroxides (LDHs) [23]. Their synthetic methodologies, mod-

* Corresponding authors.
E-mail addresses: wguo@hust.edu.cn (W. Guo), byxia@hust.edu.cn (B.Y. Xia).

https://doi.org/10.1016/j.cclet.2021.09.034
1001-8417/

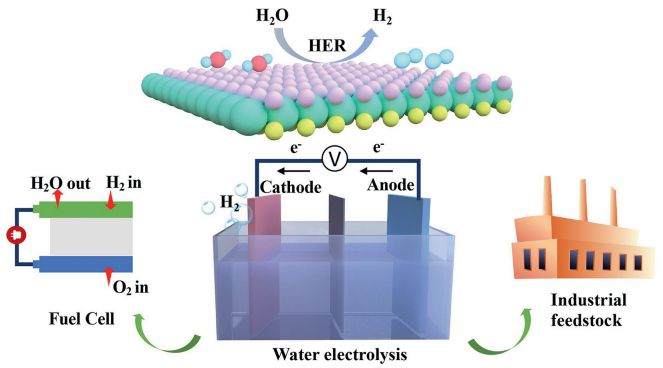

Fig. 1. Hydrogen production by electrolysis of water splitting.

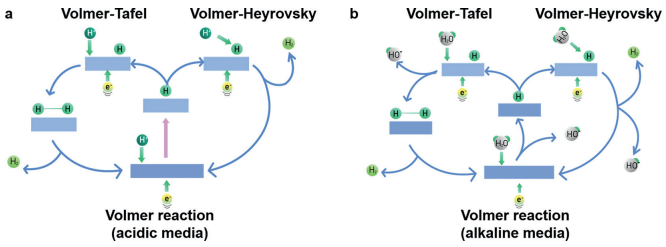

Fig. 2. Mechanism of HER on the surface of 2D materials in (a) acidic and (b) alkaline media.

ification strategies, and reaction mechanisms are summarized in this specific section. Finally, perspectives regarding the furtherance of this blossoming field are proposed. We hope this review will provide a comprehensive understanding of 2D nanocatalysts for electrochemical HER, which could promote the development of hydrogen energy technologies towards sustainable human society (Fig. 1).

2. Fundamentals of HER

2.1. Reaction mechanism

Electrochemical HER is the cathodic reaction of water electrolysis in acidic or alkaline media, where three possible elementary steps are involved. The HER occurred in acidic media can be depicted by two serial steps (Fig. 2a). It begins with the electrochemical adsorption of hydrogen (H_{ad}) on electrode surface (Eq. 1, Volmer step). The immobilized hydrogen species are derived from the combination of free electrons and proton donors, *i.e.*, hydronium ions (H_3O^+) in acidic electrolyte. Subsequently, hydrogen gas can be generated following the desorption process, where another proton binds to H_{ad} and is reduced by another free electron (Eq. 2, Heyrovsky step), or/and the coupling of two H_{ad} (Eq. 3, Tafel step) [24,25].

$$H_3O^+ + M + e^- \rightarrow M\text{-}H_{ad} + H_2O \text{ (Volmer step)} \quad (1)$$

$$H^+ + M\text{-}H_{ad} + e^- \rightarrow H_2 + M \text{ (Heyrovsky step)} \quad (2)$$

$$2M\text{-}H_{ad} \rightarrow H_2 + 2M \text{ (Tafel step)} \quad (3)$$

Akin to the reaction in acidic media, the HER occurred in alkaline media is composed by two crucial steps (Fig. 2b): the first one is generation and immobilization of H_{ad} (Eq. 4, Volmer step) and the second one is desorption process of H_2 evolution. Unlike in acidic electrolyte, the proton donors in alkaline electrolyte are obtained from the dissociation of H_2O molecules. The absorbed H_{ad} can be conducted *via* Heyrovsky step (Eq. 5, Heyrovsky step) or Tafel step (Eq. 6, Tafel step) and both to yield H_2 [26].

$$2H_2O + M + 2e^- \rightarrow 2M\text{-}H_{ad} + 2OH^- \text{ (Volmer step)} \quad (4)$$

$$H_2O + 2M\text{-}H_{ad} + e^- \rightarrow M + H_2 + 2OH^- \text{ (Heyrovsky step)} \quad (5)$$

$$2M\text{-}H_{ad} \rightarrow H_2 + 2M \text{ (Tafel step)} \quad (6)$$

2.2. Evaluation criteria of HER catalysts

2.2.1. Volcano plot

According to the Sabatier principle, the interaction between HER electrocatalysts and intermediates (H_{ad} and H_2) should be appropriate [25]. Fast H_{ad} adsorption and H_2 desorption facilitate the HER kinetics. From the physicochemical points of view, the H_{ad} adsorption and H_2 desorption can be evaluated by Gibbs free energy. The function between the experimentally measured exchange current density (j_0) of HER and the calculated Gibbs free energy (ΔG_{H^*}) of the adsorbed hydrogen atoms on various metals can be plotted (Fig. 3a) [25]. This proposed "volcano-type" plot defines the best HER activity at the top with $\Delta G_{H^*} = 0$, where the catalytic performance of Pt metal is identified to be prior to others. It also provides a strong theoretical basis for evaluating the kinetic activity of the catalysts [27]. With the development of computational science and theoretical calculations, more valuable information of ΔG_{H^*} about HER electrocatalysts have been achieved [28].

2.2.2. Overpotential

Basically, the reaction of water splitting in the electrochemical cell can start with a Nernst potential under the ideal standard temperature and pressure conditions. However, a greater potential is usually required in practical HER to overcome the energy barrier. The difference between practical potential and Nernst potential is called overpotential η (Fig. 3b). Consequently, the efficiency of water electrolysis is limited by the kinetic barrier for water dissociation. Minimizing the overpotential of HER is important for the further development of hydrogen economy.

2.2.3. Tafel equation

The Tafel equation can be used to describe the current-potential relationship under an apparent overpotential η, as described in Eq. 7, where j is the current density, j_0 represents the exchange current density, and b is the corresponding Tafel slope [29].

$$\eta = b\log(j/j_0) \quad (7)$$

The Tafel slope b represents the potential difference required to increase or decrease the current density tenfold. The HER reaction mechanism can be inferred through the experimentally measured Tafel slope [30].

The exchange current density j_0 is another important kinetic parameter in HER, which determines the electrochemical reaction rate under a certain applied potential (Fig. 3c) [27]. The ideal electrocatalysts with minimized Tafel slope and high exchange current density are taken together suggesting favorable reaction kinetics for electrochemical HER [31,32].

2.2.4. Stability

The stability refers to the activity evolution of the catalyst over time. Because the electrocatalysts may experience chemical or structural alterations during operational use. Inadvertently, their stability in HER may be affected. Thus, measuring the electrocatalyst stability is important. The chronopotentiometry (current-time curve) or chronoamperometry (potential-time curve) and repetitive

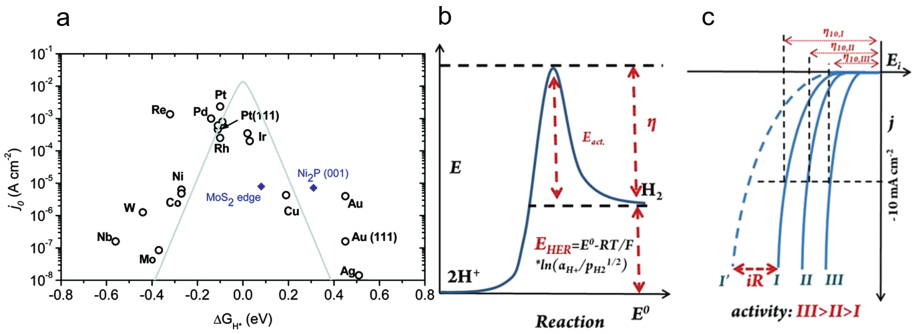

Fig. 3. (a) A volcano plot of experimentally measured exchange current density as a function of ΔG_{H^*}. Reproduced with permission [25]. Copyright 2014, the Royal Society of Chemistry. (b) Schematic illustration of the HER energetics. Reproduced with permission [27]. Copyright 2019, Wiley-VCH. (c) Schematic HER polarization curves on different electrocatalysts. Reproduced with permission [27]. Copyright 2019, Wiley-VCH.

cyclic voltammetry (CV) measurements are usually used for evaluating the stability [33]. In the former two methods, a current density of 10 mA/cm^2 is commonly applied as the descriptor, the catalytic stability can be assessed by the current or potential decay during the durability test. As for the CV test, the stability is evaluated by comparing the polarization curves before and after a continuous CV cycle (usually 500–10,000 cycles).

2.2.5. Faradic efficiency

Faradaic efficiency (FE) describes the efficiency of charge transfer for target reaction in an electrochemical reaction system, which dictates the selectivity of electrocatalysts. FE is defined as the ratio of effective charge transfer to the total charge consumed in HER. The HER electrocatalyst with ideal FE can increase the productivity of H_2 and eliminate the extra cost of product separation and purification. Generally, the actual H_2 output measured by gas chromatography or water gas displacement method is compared with the theoretical H_2 output calculated by constant current or constant potential electrolysis to calculate the FE of HER [34].

3. 2D electrocatalysts for HER

2D materials have diversified in many applications dictated by their unique atomic structure and intrinsic physical properties. The allure of 2D electrocatalysts in HER can be mapped to three aspects including specific surface area, 2D planer structure and electronic conductivity. 2D materials have maximal surface to bulk ratio, providing abundant active sites for hydrogen adsorption, and the atomically thin thickness guarantees the rapid transfer of free electrons. Besides, the open 2D planes can be directly modified by heteroatom doping, defect engineering, surface functionalization, and composite construction, resulting in enhanced electrochemical HER performance. The 2D electrocatalysts are classified into organic composites, such as metal organic frameworks (MOFs), covalent organic frameworks (COFs); and inorganic nanocatalysts, including metallic nanomaterials, metal-free nanomaterials, transition metal dichalcogenides (TMDs), MXenes and layered double hydroxides (LDHs). The corresponding synthetic protocols, modification strategies, and structure-performance relationship are discussed below.

3.1. 2D organic materials

2D organic materials possess a periodic network of repetitive organic units arranged along two orthogonal directions in an isolated sheet structure, which endows them outstanding advantages including molecular diversity and adjustable functionality [35,36]. The MOFs, COFs and a variety of their modified derivatives, are efficient electrocatalysts for HER.

3.1.1. Covalent organic frameworks (COFs)

The COFs are generally assembled by strong covalent conjunction between light elements such as carbon, nitrogen and oxygen with reticular arrangement [37]. The intimate interlayer electronic interactions within the porous COFs structures ensure the high electrical conductivity and facile electron migration across abundant catalytic sites, which make them promising catalysts in electrochemical HER [38–40]. Chen group reported porphyrin-based COF nanosheets for electrochemical HER in 1 mol/L KOH, with an overpotential of 398 mV and a small Tafel slope of 161 mV/dec, as well as the slight current attenuation (16.4%) after chronopotentiometry test for 10 h. The linkage between active centers of COF and butadiyne facilitates the charge migration across the electrode-electrolyte interface thus promotes the progress of HER (Fig. 4a) [41]. However, the lack of active sites in pristine 2D COFs limits the catalytic performance. Theoretical studies by Ball *et al*. proved that the bipyridine-linked co-doped COFs with heteroatoms of silicon and phosphorus manifested facile charge transfer kinetics and desirable hydrogen atom adsorption Gibbs free energy (Fig. 4b) [42]. Doping with metal species also augments HER activity. Maiti *et al*. prepared Ru doped COFs with a positive onset potential of 159 mV in 1.5 mol/L H_2SO_4 and remarkable stability with negligible change of exchange current density and polymeric framework after 100 cycles. The incorporation of Ru increases the flexibility of the COFs structure and accelerates charge transfer (Fig. 4c) [43]. Besides, the heteroatom-doped COFs are promising precursors for fabricating heteroatom-doped carbon-based electrocatalysts [44]. Such COF-derived carbon materials have a spectrum of uniformly dispersed active sites, excellent stability, ordered porous and covalent conjunction structure, all of which are favorable merits for HER [45].

3.1.2. Metal organic frameworks (MOFs)

The MOFs with metal centers immobilized by organic ligands are an emerging class of porous layered materials. The tailorable nature by replacing the coordinated metal sites or organic linkers makes the ideal candidates in diverse heterogeneous catalytic processes (Fig. 4d) [46–48]. The MOFs in possession of porous structure, abundant metal active sites and excellent electrical conductivity, are another group of potential catalysts for HER [49–51]. Compared with single-metal center MOF catalysts, the bimetallic center MOF catalysts have more active sites. The synergistic effects between the bimetallic metal nodes can accelerate the reaction kinetics [52]. While the pristine MOFs suffer from high overpotential, hybrid MOF-based electrocatalysts have outstanding efficiency in HER originating from the synergistic effect between MOFs and foreign materials, as a result of optimized ΔG_{H^*} of the intermediate products, improved electrical conductivity, enhanced intrinsic catalytic activity and increased number of active sites [53].

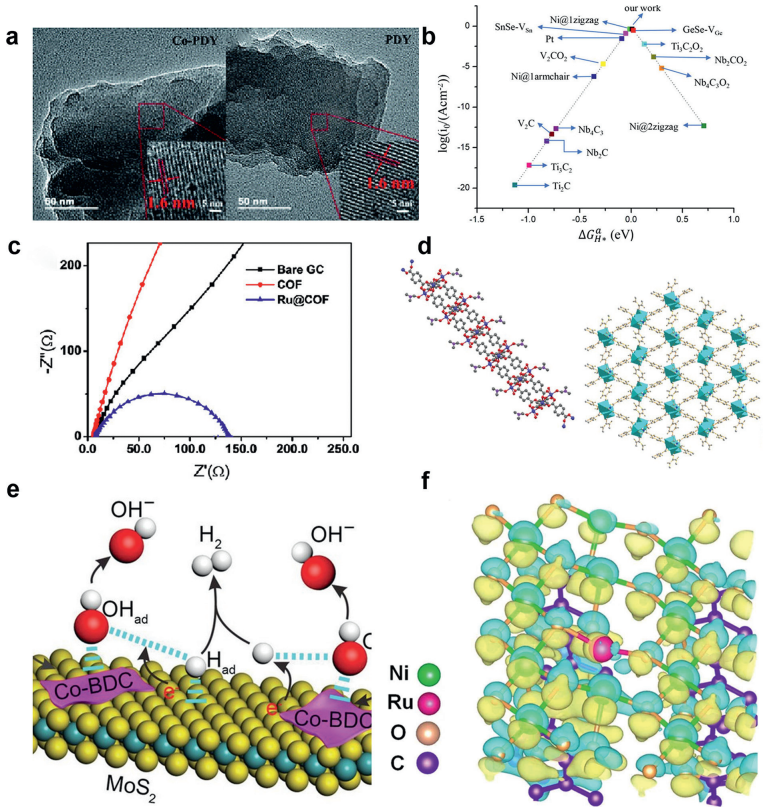

Fig. 4. (a) The TEM images of Co-COF and COF. Reproduced with permission [41]. Copyright 2019, the Royal Society of Chemistry. (b) Volcano plot of the average ΔG_{H^*} values of different catalysts. Copied with permission [42]. Copyright 2020, American Chemical Society (c) Impedance curves of the COF and Ru@COF. Copied with permission [43]. Copyright 2020, Wiley-VCH. (d) The structure of the MOF composing of CoO_6 octahedra coordinated in a plane to ligands. Reproduced with permission [46]. Copyright 2019, Wiley-VCH. (e) The catalysis mechanism of HER in alkaline solution on the Co-MOF/MoS_2 nanosheets. Copied with permission [54]. Copyright 2019, Wiley-VCH. (f) The charge density of Ni-BDC and $NiRu_{0.13}$-BDC. Reproduced with permission [57]. Copyright 2021, Springer Nature.

Zhu *et al.* reported the novel Co-BDC ($C_8H_4O_4$)/MoS_2 hybrid nanosheets from a facile sonication-assisted solution method, with an onset overpotential of only 155 mV and negligible potential shift of the polarization curve after 2000 CV cycles in Ar-saturated 1.0 mol/L KOH solution [54]. The MOF nanosheets facilitate the adsorption and dissociation of H_2O molecules to provide abundant protons for the adjacent MoS_2. Subsequently, the MoS_2 nanosheets provide essential reaction active sites for H_2 desorption and generation (Fig. 4e). Adding conductive materials or introducing extra metallic sites is another choice for optimizing the HER performance of MOF-based electrocatalysts [51,55,56]. Sun *et al.* introduced Ru single atoms into MOF materials, which exhibited a low overpotential of 36 mV at the current density of 10 mA/cm^2 in 1 mol/L phosphate buffered saline solution. A tiny current decrease was observed after 30 h test and the faradic efficiency was estimated to be approximately 100% [57]. The dispersed Ru atoms provide extra active sites, and further modulate the electronic structure of the active centers for better H_2O and H* adsorption (Fig. 4f). Likewise, Dong *et al.* selectively doped the molecular metal dithiodiamine into MOFs and gained the best performance among the same type of catalysts in 0.5 mol/L H_2SO_4 solution [58]. The integration of homogeneous metal complexes and heterogeneous MOFs enriches the catalytic active sites, as well as optimizes the adsorption and desorption energy of H through the strong coordination interaction. Akin to above mentioned COF materials as precursors for heteroatom-doped carbon catalysts, various metal-carbon catalysts with heteroatoms can derive from MOFs, such as single-metal/bimetallic-based electrocatalysts, metal oxides/sulfides electrocatalysts and their hybrids [59–61].

3.2. 2D inorganic materials

2D inorganic electrocatalysts have many unique physicochemical properties, especially large surface area, short ion and charge transfer path, flexible and controllable compositions and structures, ultra-thin thickness and easy functionalization, which make them promising candidate materials for HER [62,63]. In addition to the inorganic 2D metal-carbon hybrid composites derived from their corresponding MOF precursors, there are a wide variety of 2D inorganic electrocatalysts for electrochemical HER encompassing 2D metallic nanomaterials, 2D metal-free material, MXenes, TMDs and LDHs, as discussed in the following sections.

3.2.1. 2D metallic nanomaterials

Recently, emerging 2D metallic nanomaterials composed of bare metal elements of multiple atomic sizes have attracted more attention and enriched the diversity of 2D materials [64]. 2D metal nanomaterials can be prepared through various methods, such as organic ligand-assisted growth, small-molecules-and-ions-mediated synthesis, 2D template-confined synthesis, seeded growth, photochemical synthesis, hydrothermal/solvothermal synthesis and exfoliation (Fig. 5a) [64,65]. 2D metal nanosheets are potential candidates as hydrogen evolution catalysts owing to their innate electrical conductivity and electrochemical stability [64,66,67]. However, the current research of such electrocatalysts is limited in noble metals [68,69]. Other electrocatalysts from earth-abundant metals need to be developed. Li *et al.* constructed IrRh metal nanosheets with an astonishingly low overpotential of 35 mV at current density of 10 mA/cm^2 in 1.0 mol/L KOH solution, outperforming the commercial Pt/C catalysts (46 mV) (Fig. 5b). The

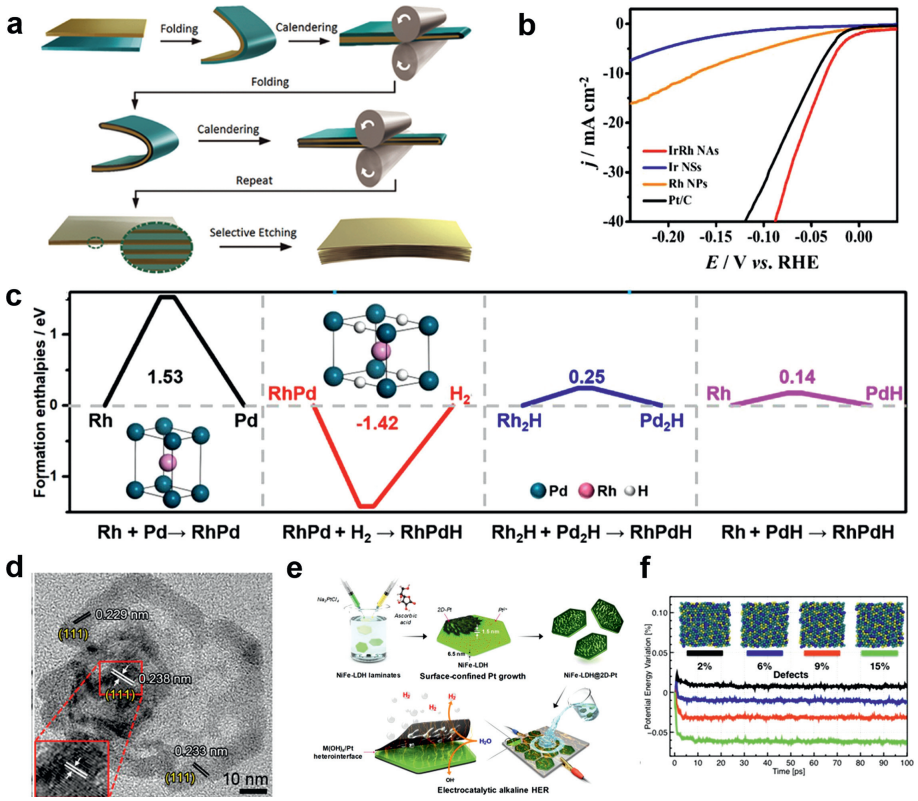

Fig. 5. (a) Schematic showing of the fabrication of metal nanosheets. Copied with permission [65]. Copyright 2016, Wiley-VCH. (b) HER polarization curves for different catalysts. Copied with permission [70]. Copyright 2019, American Chemical Society. (c) The formation enthalpies values of RhPd and RhPd-H. Reproduced with permission [71]. Copyright 2020, American Chemical Society. (d) The HRTEM image of PtAgCo nanosheets. Reproduced with permission [72]. Copyright 2017, American Chemical Society. (e) Schematic representation for 2D-Pt on LDH synthesis and its application. Copied with permission [73]. Copyright 2020, American Chemical Society. (f) 2D suspended 10-fold material with quantities of defects in difference. Reproduced with permission [74]. Copyright 2019, American Chemical Society.

electronic structure effect between Ir and Ru helps optimize the adsorption states and charge transfer properties [70].

The catalytic performance of bare bimetallic nanosheets can be further improved by heteroatom doping with additional catalytic sites and altered the electronic structure. Fan *et al.* introduced H atoms into bimetallic RhPd nanosheets, resulting in a prominently low overpotential of 40 mV and predominant stability for over 10 h at 100 mA/cm^2 in 1 mol/L KOH solution. The confined H stabilizes the RhPd nanosheets bimetallene and enhances the activity (Fig. 5c) [71]. Mahmood *et al.* prepared ultrathin porous PtAgCo nanosheets by doping Co into PtAg alloy. The Co atoms change the electronic structure of the PtAg alloy and contribute to the desorption of H_{ad} by downshifting the Fermi level of PtAg (Fig. 5d) [72].

Loading porous Pt nanosheets onto nickel hydroxide iron sheets leads to fast charge migration and diffusion of electrolyte ions at an intimate 2D-2D interface (Fig. 5e) [73]. Yadav *et al.* combined 2D Al alloys in 2-fold decagonal quasicrystalline symmetry with WS_2, forming a heterostructure with stack faults (Fig. 5f), as a result of enlarged the active areas. The hybrid catalyst manifested a low overpotential of 60 mV and long-term stability in the solution of 0.5 mol/L H_2SO_4 [74]. It is worthy noting that fabricating 2D metallic material-based composite can reduce the capital cost. This is expected to be applied in large-scale industry.

3.2.2. 2D metal-free alkenes

Graphene is defined as a 2D honeycomb planar monolayer of carbon atoms with outstanding physical and chemical properties [75,76]. While pristine graphene is electrochemically inert and exhibits negligible HER activity over a stable and large window. Chemically modified graphene, has been verified to exhibit improved electrocatalytic HER performance. For example, a suitable ΔG_{H^*} of 0.08 eV for the initial H* adsorption could be obtained over the N, P co-doped graphene (Fig. 6a) [18]. Hu *et al.* proposed the proton-penetration process over N-doped graphene wrapped NiCu bimetallic sheets. The number of the covered graphene layers were closely related to the HER activity of the catalyst. The penetrating ability of protons determined the HER activity. The graphene-cover strategy can also prevent the metal nanoparticles from corrosion in strong alkaline environment (Fig. 6b) [77]. Moreover, the graphene matrix composites by coupling alternating active MoS_2 with reduced graphene oxides layers showcased excellent catalytic activity with a low onset overpotential of 140 mV and a large current density of 23 mA/cm^2 at 200 mV in 0.5 mol/L H_2SO_4. The outstanding catalytic HER performance of MoS_2/graphene composites descends from the sufficiently high exposure of active edge sites and high conductivity of graphene substrate [78].

Black phosphorus (BP) is a layered semiconductor composed of corrugated planes of phosphorus atoms with strong interlayer chemical bonding, high mobility, tunable band gap, large active surface area and abundant reserves on earth [79–81]. The honeycomb structure of BP can help to expose the lone pair electrons of metals. This strong activation effect of BP on metal atoms can improve the HER activity. Wang *et al.* bonded BP to Pt with an optimal ΔG_{H^*} of −0.02 eV, approximately towards to zero. This arose from the strong Pt-P interaction and remarkable durability of Pt-P bonds [82]. Li *et al.* further introduced Ru metal to BP-Pt catalyst, which exhibited greatly enhanced HER activity with a prominent overpotential of 22 mV at 10 mA/cm^2 in a 1 mol/L KOH solution, much lower than that of commercial Pt/C (77 mV) and Pt NCs/BP (64 mV). The electrons accumulate on the hybrid interface, leading to shortage of electrons on Ru. Thus, the Ru atoms are favorable

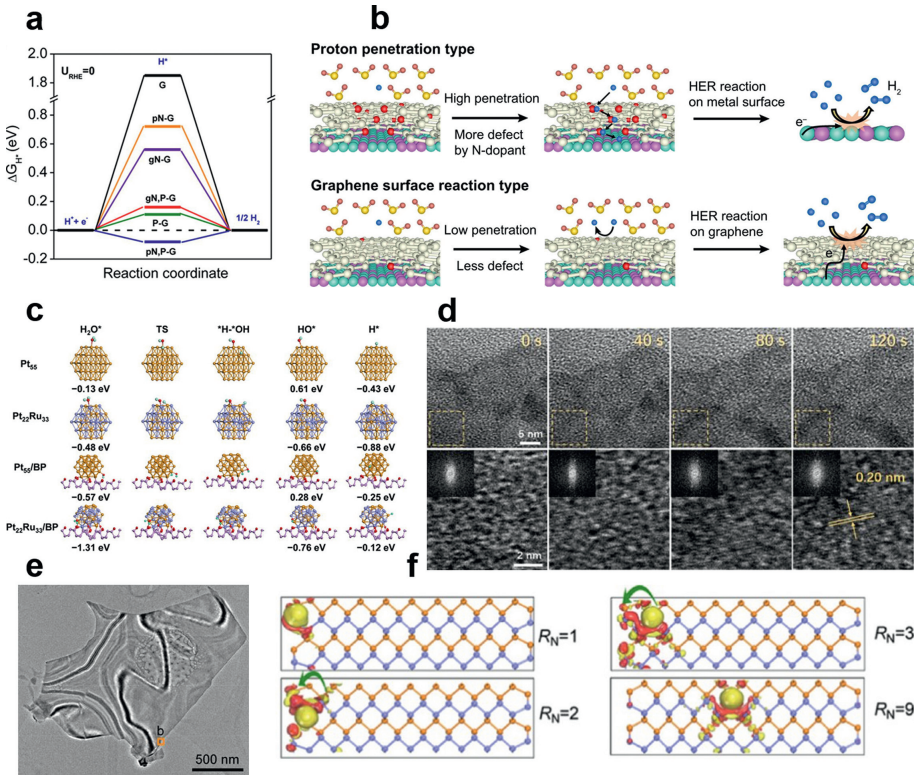

Fig. 6. (a) Calculation of ΔG_{H^*} values for N- and/or P-doped graphene. Reproduced with permission [18]. Copyright 2014, American Chemical Society. (b) Probable HER mechanisms for graphene-covered metal catalysts. Copied with permission [77]. Copyright 2021, Springer Nature. (c) The atomic structures of H_2O, H–OH, HO, and the corresponding adsorption free energies of different catalysts. Reproduced with permission [83]. Copyright 2019, American Chemical Society. (d) *In-situ* HR-TEM images of CoFeO@BP during HER. Copied with permission [84]. Copyright 2020, Wiley-VCH. (e) TEM image of a typical MoS_2-BP nanosheet. Reproduced with permission [85]. Copyright 2017, American Chemical Society. (f) Charge transfer which induces a bound donor-defect complex between hydrogen and armchair edge. Reproduced with permission [86]. Copyright 2019, American Chemical Society.

to the electron-rich H_2O^* and HO* species, resulting in moderate binding strength (Fig. 6c) [83].

In addition, the BP could be a splendid substrate or modifier for constructing composite electrocatalysts, of which the electronic structure and conductivity of the hybrids can be tuned. For example, the CoFe oxide grown on BP substrate *via* a facile solvothermal strategy, exhibiting an overpotential of 88 mV at 10 mA/cm^2 in 1 mol/L KOH solution. The metastable amorphous CoFe oxide can be turned to different active states during redox reactions and CoFe phosphides can be formed on BP substate as active centers of HER (Fig. 6d) [84]. Similarly, He *et al.* deposited active MoS_2 on BP to construct a MoS_2-BP heterogeneous interface (Fig. 6e). The hybrid catalyst exhibited an overpotential of 85 mV at 10 mA/cm^2 and less than 3% degradation of current density after 10,000 s in the media of 0.5 mol/L H_2SO_4. The electrons accumulated on MoS_2 promote the coupling of electrons and protons at the catalyst-electrolyte interface, accelerating electron and mass transfer. Hence the kinetic barrier of elementary reactions is reduced [85]. Besides, density functional theory calculations affirmed that the fabrication of vacancies can effectively accelerate charge transfer and improve the inherent catalytic activity of BP, which is important for designing BP with high electrocatalytic activity (Fig. 6f) [86].

3.2.3. Transition-metal dichalcogenides (TMDs)

As binary analogues to graphene, TMDs have the general molecular formula of MX_2, where M is a transition metal belonging to groups IVB to VIIIB and X is a chalcogen from group VIA (S, Se, Te). The M and the X are connected by a strong ionic bond. The crystal structure of 2D TMD consists of a X-M-X sandwich model with van der Waals interactions. TMDs have suitable aspect ratio structures and tunable layer-dependent electronic structure [87]. Through the different ways of interlayer X-M-X layer stacking, the chemical phase of MX_2 can be divided into triangular (1T), the distorted 1T (1T') and hexagonal (2H) (Fig. 7a). 1T-phase TMDs possess metallic properties such as higher electrical conductivity, which is more beneficial to electrocatalytic HER. The unique phase transformation properties of TMDs open up a novel avenue to the rational design of high-efficiency electrocatalysts for HER [88].

Molybdenum disulfides (MoS_2) have been widely studied as electrocatalysts since 1970s [89], with edge sites proved to be active for HER [90]. As the development of size and morphology control of MoS_2 [91–93], the Mo with 50% sulfur content was found to be the optimal edge surface [94]. HER activity showed a linear correlation with the length of edge on MoS_2 catalyst. (Fig. 7b) [95]. Furthermore, studies have suggested that the HER activity is also essentially determined by the electronic structure of TMDs, which can be optimized by phase engineering, heteroatom doping, and interfacial design approaches (Fig. 7c). [96–98]. N-doped MoS_2 nanosheets from a facile self-templating method have high density of active edge sites and upgraded electronic conductivity in basal plane, exhibiting outstanding HER performance with an overpotential of 114 mV to reach 10 mA/cm^2 and long-term stability over 10 h in 0.5 mol/L H_2SO_4 [99]. Similarly, The Ni doping can effectively decrease the kinetic energy barrier of the initial step of water splitting and accelerate the desorption of the formed OH^-, displaying superior HER activity in 1 mol/L KOH aqueous solution with an exceedingly low overpotential of ~98 mV at 10 mA/cm^2 [100–103]. Besides, optimizing the reaction interface of MoS_2 to preferentially adsorb reactants to inner Helmholtz plane is able to efficiently reduce kinetic resistance of HER. Luo *et al.* constructed a di-anionic MoS_2 surface by OH^-, which possessed controlled molecular substitution of S sites that were functioned as active

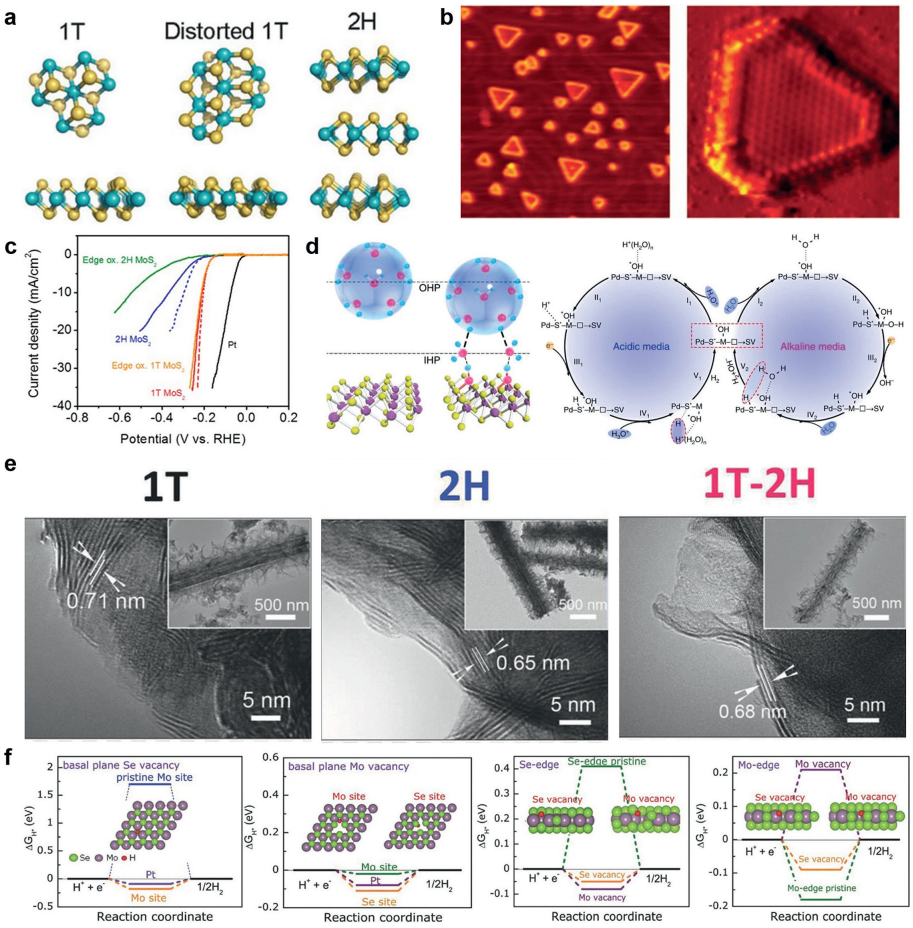

Fig. 7. (a) Schematic structures of MoS_2 with different phases of 1T, distorted 1T, 2H. Reproduced with permission [88]. Copyright 2017, American Chemical Society. (b) STM images of MoS_2 nanoparticles on Au (111). Reproduced with permission [95]. Copyright 2007, American Association for the Advancement of Science. (c) Polarization curves of different phase states of MoS_2 nanosheet electrodes before and after edge oxidation. Reproduced with permission [97]. Copyright 2013, American Chemical Society. (d) Schematic illustration of OH^- functionality in upgrading HER on the di-anionic MoS_2 interface and the probable reaction processes. Reproduced with permission [104]. Copyright 2020, Springer Nature. (e) TEM-HRTEM images and SAED patterns of different $MoSe_2$ nanosheets. Reproduced with permission [102]. Copyright 2018, Wiley-VCH. (f) The calculated results of HER free energy and ΔG_{H^*} with Mo site and Se site in different cases. Reproduced with permission [111]. Copyright 2018, Wiley-VCH.

sites. Furthermore, the OH^- modified on the MoS_2 interface endows strong non-covalent hydrogen bonding effect with the reactants (Fig. 7d) [104]. Similar studies were also noted for ReS_2, VS_2, RuS_2, WS_2 and other transition metal-dithio compounds [105–107].

Akin to MoS_2, $MoSe_2$ has excellent HER performance [108]. The 1T-$MoSe_2$ is better than 2H-$MoSe_2$ because of much more predominant active area and higher conductivity [109]. Deng *et al.* designed a stable (1T-2H)-$MoSe_2$ through phase modulation and N-doping method to achieve efficient HER performance with a notably low overpotential of 137 mV at 100 mA/cm^2 and a small Tafel slope of 32 mV/dec in a 0.5 mol/L H_2SO_4 electrolyte. The N doping can offer more electrochemical active areas, high electrical conductivity, and promote the phase transition from 2H to 1T (Fig. 7e) [102]. Chen *et al.* doped Co into $MoSe_2$ to build a heterogeneous catalyst *via* chemical vapor deposition method. The Co dopants help to generate more distortions and defects, which consequently introduce more active sites and eventually boost the HER performance [110]. Except doping approaches, designing vacancies is also a potential strategy to increase active sites and stimulate intrinsic catalytic activity [101]. The feasibility of defect engineering has been demonstrated by introducing Se and Mo vacancies into $MoSe_2$. The Se and Mo vacancies can regulate the electronic structure of the basal plane and edge, thereby optimizing the ΔG_{H^*} to nearly zero and generating more catalytic sites (Fig. 7f). Meanwhile, the Se and Mo vacancies are expected to increase the number of gap states and the density of electrons near the Fermi level, as a result of reduced kinetic barrier of HER in 0.5 mol/L H_2SO_4 media [111].

3.2.4. MXenes

MXenes in possession of excellent electrical conductivity and more catalytically active sites are potential substitutions of 2D metal-free alkene and TMDs for electrochemical HER [112]. The general formula of MXene is $M_{n+1}X_nT_x$, where M stands for an early transition metal, X can be C or N, and T_x is the surface functional group O, OH or F [113]. Generally, most of the MXenes are prepared from selective chemical etching of layered materials $M_{n+1}AX_n$ (A are main group elements such as Al) with HF, NH_4HF_2 or LiF/HCl mixtures [114]. W_XC is predicted to have the highest catalytic activity among other Mxenes, according a calculated ΔG_{H^*} that is closest to 0 eV. However, this is not experimental documented because of its poor stability, high density covered F groups and unskillful preparation methods [115,116]. The HER catalytic activity of MXenes also can be upgraded *via* defect engineering by adding ad-atoms or vacancies. Lind *et al.* studied the vacancy effect on the HER performance of $W_{1.33}C$. They found that protons can transfer to the vacancies and transform to hydrogen atoms under a metastable condition at high cathodic potentials (Fig. 8a) [117]. Similarly, the $Mo_2TiC_2T_x$ nanosheets with a large number of surface Mo vacancies derived from electrochemical exfoliation can im-

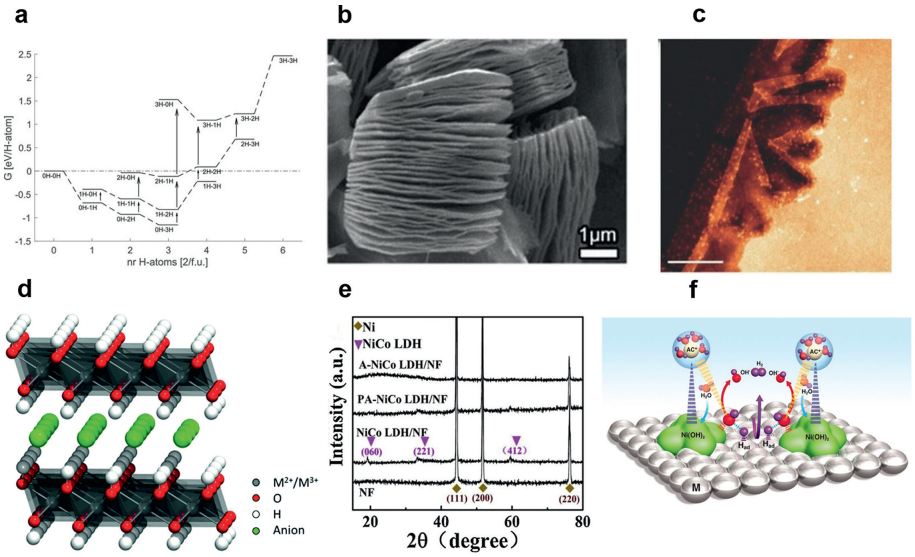

Fig. 8. (a) A landscape of relative energies of all configurations of adsorbed H on $W_{1.33}C$. Copied with permission [117]. Copyright 2021, Wiley-VCH. (b) The SEM image of $Ti_3C_2T_x$ nanosheets. Reproduced with permission [119]. Copyright 2019, Wiley-VCH. (c) The STEM-ADF image of an edge region in Mo_2C film. Reproduced with permission [122]. Copyright 2017, Wiley-VCH. (d) The schematic structure of LDH. Copied with permission [126]. Copyright 2021, the Royal Society of Chemistry. (e) The XRD patterns of different materials. Copied with permission [127]. Copyright 2017, the Royal Society of Chemistry. (f) Schematic representation of formation of various bonds on the surface of the catalyst. Copied with permission [26]. Copyright 2011, American Association for the Advancement of Science.

prove the hydrogen absorption and desorption characteristics with low overpotentials of 30 and 77 mV at 10 and 100 mA/cm^2 in a 0.5 mol/L H_2SO_4 media, respectively [118].

The unique interface functional groups of MXenes are of vital importance to electrocatalysis performance. Thus, surface functionalization, such as oxidation and hydrogenation can improve the inherent activity adsorption ability of the reaction intermediates of the MXenes catalyst [115]. Jiang *et al.* reported the oxygen-functionalized ultrathin packed accordion-like $Ti_3C_2T_x$ nanosheets with a low overpotential of 190 mV at 10 mA/cm^2 in a 0.5 mol/L H_2SO_4 electrolyte (Fig. 8b) [119,120]. Besides, hydrogenated MXenes also displayed improved HER performance due to the increased density of covered H atoms on the surface of catalysts, which endowed minimized overpotential and near-zero ΔG_{H^*} [115].

Furthermore, MXenes coupled with other materials can increase the number of active sites and conductivity. Xiao *et al.* fabricated a heterostructure of highly conductive $MoSe_2$ and oxygen-terminated Ti_3C_2, as a result of accelerated charge transfer and reduced surface reaction kinetics [121]. In addition, Geng *et al.* fabricated a vertically large-area Mo_2C/graphene integrated structure with high crystallinity and excellent electronic coupling, which can be used as a charge relay system for HER (Fig. 8c) [122]. The integration of MXenes and the atom-thin 2D electrocatalyst is beneficial to overcome the interfacial Schottky barrier, thereby increasing the catalytic activity for HER [123,124].

3.2.5. Layered double hydroxides (LDHs)

The general formula of LDHs is $[M^{2+}_{1-x}M^{3+}_x(OH)_2]^{x+}[A_{p-x/p}]^{x+}\cdot mH_2O$, where the M^{2+} and $M^{3+}$are bivalent and trivalent metallic cations, respectively (Fig. 8d). The A^{n-} represents an interlayer anion. X is the depiction of surface charge, which is subject to change for various applications [125–127]. Many high-performance 2D electrocatalysts are suitable in acidic media. In contrast, the LDHs have commendable adaptability in various alkaline media [128,129]. The active areas of LDHs were usually buried inside or covered, leading to low inherent catalytic activity under alkaline environment. To solve this problem, Yang *et al.* fabricated vertically oriented array of noble metal-free Ni-Co LDH nanosheets doped by B, with low overpotentials of 151, 286 and 381 mV at large current densities of 100, 500 and 1000 mA/cm^2 in 1 mol/L KOH solution, respectively. The improved electrocatalytic activity could be attributed to the deconstruction of the original crystalline structure, which is caused by the BO_3^{3-} displacing the lattice OH^- in LDH (Fig. 8e). This created more effective defects such as oxygen vacancies and unsaturated atoms, and finally increased the number of electrocatalytic active sites and enhanced its conductivity. Besides, the B dopants can raise the local electron density, advance the dissociation of absorbed H_2O and transfer absorbed H onto the neighboring metal atoms to produce H_2 [130]. Similarly, doping on a 2D single-layer $Ni(OH)_2$ with platinum nanowires exhibited excellent electrocatalytic activity for HER in an alkaline solution with a low potential of −0.07 V at 2.48 mA/cm^2. In this hybrid system, $Ni(OH)_2$ substrates can effectively activate the HO–H bond, improving aqueous solubility of the catalyst (Fig. 8f) [26]. Besides, the unique 1D-2D ultrathin structure of the catalyst can expose more active areas, while improve the rate of electron transporting and lower dynamic barrier of Volmer step. The large contact area between Pt and LDH can effectively reduce any possible migration and aggregation, thus enhancing the catalytic stability [131].

4. Conclusions and perspectives

This comprehensive review summarized the recent advances of high-performance HER 2D electrochemical nanocatalysts. The corresponding strategies for engineering the catalytic performance are introduced. We shed light on the inherent electrochemistry arising from intrinsic elemental make-up, and upgraded performance by physical and chemical modifications, such as doping, defect, and phase engineering, as well as fabricating composites with different building blocks. Despite the significant progress has been achieved so far, the fundamental research and practical large-scale application of hydrogen energy fed by electrochemical hydrogen evolution are still in a developing stage. Many critical challenges still remain around the future landscape of this important research topic (Fig. 9).

First, there have been significant progress and breakthrough in development of high-performance 2D electrocatalysts. It is desirable to achieve better HER catalysts superior to commercial Pt/C

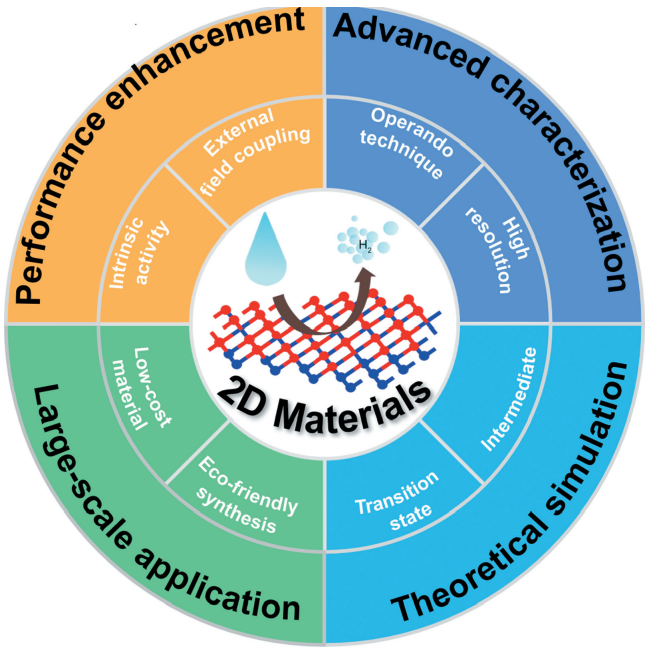

Fig. 9. Panoramic prospects of 2D electrocatalysts for HER.

electrocatalyst. Despite enriching the family with more 2D electrocatalysts and modification strategies, some external field coupling could be considered, such as electric field, magnetic field, vibration and light illumination. They can adjust the intrinsic activity of the catalyst and provide additional driving forces to improve the reaction dynamics [132,133].

Second, many ambiguities still remain regarding the reaction mechanism of HER. Current characterizations of HER only provide the information before and after HER measurements while important information such as intrinsic structure evolution and absorbed intermediates during reaction is missing. Unfortunately, these are more essential for understanding the HER mechanism. Thus, the development of more operando characterization and high-resolution techniques to probe the active sites and the microstructure of electrocatalysts during the HER process is highly desirable to unveil the underlying catalytic mechanism, especially for hybrid 2D electrocatalyst systems.

Third, currently used density functional calculations have been widely employed to predict HER transition states and intermediates. Most of time, it is not convincing enough to support the hypothesis implying from experimental results. Gaining insight into the mechanisms of HER is also beneficial for rationally guiding the design of high-performance catalysts. To date, the flourishment of artificial intelligence has made it possible to conduct automatic calculation and online simulation [134]. The mechanistic knowledge derived from these tools could be fed back to the active machine learning to screen the desirable candidates for experimental validation.

Finally, the electrochemistry of 2D materials provides opportunities to discover their practical application in energy catalysis. Their capital cost and green-chemistry synthetic methods should be on the list of priorities. To expand the production from lab "hand-made" to industrial scale ones, low-cost materials and eco-friendly synthesis approches should be explored. Moreover, the electricity consumption of water electrolyzers cannot be neglected. Efficient anode materials, and alternative fine chemicals refinement reaction, coupled with these effective cathodic HER catalysts powered by the renewable electricity resource could be utilized to bloom the industrial-scale hydrogen production.

In summary, the advance of extensive and in-depth researches on 2D materials make them a type of valuable catalyst in electrocatalytic hydrogen production. In view of their successful experience in electrocatalytic HER, the utility of 2D nanocatalysts could be extended in many other electrochemistry-related industries such as photocatalysis, batteries, semiconductors, biosensing and healthcare. The ultimate goal of sustainable development of human society will probably be achieved.

Declaration of competing interest

The authors declare that they have no known competing financial interests or personal relationships that could have appeared to influence the work reported in this paper.

Acknowledgments

This work was supported by the National Natural Science Foundation of China (Nos. 22075092, 21805103), the Program for HUST Academic Frontier Youth Team (No. 2018QYTD15), the Innovation and Talent Recruitment Base of New Energy Chemistry and Device (No. B21003) and the National 1000 Young Talents Program of China.

References

[1] Q. Xu, J. Zhang, D. Wang, Y. Li , Chin. Chem. Lett. 32 (2021) 3771–3781.
[2] Y. Wang, Y. Zhao, X. Ding, L. Qiao, J. Energy Chem. 60 (2021) 451–479.
[3] J. Chi, H. Yu, Chin. J. Catal. 39 (2018) 390–394.
[4] L. Zhang, L. Zhuang, H. Liu, et al., Small Sci. 1 (2021) 2000027.
[5] S. Li, J. Sun, J. Guan, Chin. J. Catal. 42 (2021) 511–556.
[6] M. Grätzel, Nature 414 (2001) 338–344.
[7] L. Zhang, H. Zhao, S. Xu, et al., Small Struct. 2 (2021) 2000048.
[8] C.T. Hsieh, X.F. Chuah, C.L. Huang, et al., Small Method 3 (2019) 1900234.
[9] C. Chen, L. Wang, B. Zhu, et al., J. Energy Chem. 54 (2021) 528–554.
[10] Y. Zhang, K. Ren, L. Wang, L. Wang, Z. Fan , Chin. Chem. Lett. 33 (2022) 33–60.
[11] H.C. Zeng, ChemCatChem 12 (2020) 5303–5311.
[12] V. Polshettiwar, R. Luque, A. Fihri, et al., Chem. Rev. 111 (2011) 3036–3075.
[13] Y. Gong, X. Xing, Y. Wang, et al., Small Sci. (2021) 2100006.
[14] H.B. Aiyappa, J. Masa, C. Andronescu, et al., Small Method 3 (2019) 1800415.
[15] X. Liu, T. Yue, K. Qi, et al., Chin. Chem. Lett. 31 (2020) 2189–2201.
[16] W. Liu, H. Zhang, C. Li, et al., J. Energy Chem. 47 (2020) 333–345.
[17] P. Prabhu, J.M. Lee, Chem. Soc. Rev. 50 (2021) 6700–6719.
[18] Y. Zheng, Y. Jiao, L.H. Li, et al., ACS Nano 8 (2014) 5290–5296.
[19] D. Liu, J. Wang, J. Lu, et al., Small Method 3 (2019) 1900083.
[20] D. Voiry, J. Yang, M. Chhowalla, Adv. Mater. 28 (2016) 6197–6206.
[21] Y. He, P. Tang, Z. Hu, et al., Nat. Commun. 11 (2020) 57.
[22] S. Intikhab, V. Natu, J. Li, et al., J. Catal. 371 (2019) 325–332.
[23] W. Fang, L. Huang, S. Zaman, et al., Chem. Res. Chin. Univ. 36 (2020) 611–621.
[24] A.J. Bard, Nature 368 (1994) 597–598.
[25] C.G. Morales-Guio, L.A. Stern, X. Hu, Chem. Soc. Rev. 43 (2014) 6555–6569.
[26] R. Subbaraman, D. Tripkovic, D. Strmcnik, et al., Science 334 (2011) 1256.
[27] Q. Gao, W. Zhang, Z. Shi, L. Yang, Y. Tang, Adv. Mater. 31 (2019) 1802880.
[28] Z.W. Seh, J. Kibsgaard, C.F. Dickens, et al., Science 355 (2017) eaad4998.
[29] B. Xiong, L. Chen, J. Shi, ACS Catal. 8 (2018) 3688–3707.
[30] J. Zhu, L. Hu, P. Zhao, L.Y.S. Lee, K.Y. Wong, Chem. Rev. 120 (2020) 851–918.
[31] H. Vrubel, T. Moehl, M. Grätzel, X. Hu, Chem. Commun. 49 (2013) 8985–8987.
[32] M. Zeng, Y. Li, J. Mater. Chem. A 3 (2015) 14942–14962.
[33] J. Wang, F. Xu, H. Jin, Y. Chen, Y. Wang, Adv. Mater. 29 (2017) 1605838.
[34] A. Ali, P.K. Shen, Carbon Energy 2 (2020) 99–121.
[35] S.L. Cai, W.G. Zhang, R.N. Zuckermann, et al., Adv. Mater. 27 (2015) 5762–5770.
[36] F. Yang, S. Cheng, X. Zhang, et al., Adv. Mater. 30 (2018) 1702415.
[37] M.X. Wu, Y.W. Yang, Chin. Chem. Lett. 28 (2017) 1135–1143.
[38] T. Sick, A.G. Hufnagel, J. Kampmann, et al., J. Am. Chem. Soc. 140 (2018) 2085–2092.
[39] S.Y. Ding, J. Gao, Q. Wang, et al., J. Am. Chem. Soc. 133 (2011) 19816–19822.
[40] H. Sahabudeen, H. Qi, B.A. Glatz, et al., Nat. Commun. 7 (2016) 13461.
[41] H. Huang, F. Li, Y. Zhang, Y. Chen, J. Mater. Chem. A 7 (2019) 5575–5582.
[42] B. Ball, C. Chakravarty, P. Sarkar, J. Phys. Chem. Lett. 11 (2020) 1542–1549.
[43] S. Maiti, A.R. Chowdhury, A.K. Das, ChemNanoMat 6 (2020) 99–106.
[44] C. Yang, S. Tao, N. Huang, et al., ACS Appl. Nano Mater. 3 (2020) 5481–5488.
[45] D. Wu, Q. Xu, J. Qian, X. Li, Y. Sun, Chem. Eur. J. 25 (2019) 3105–3111.
[46] A. Dhakshinamoorthy, A.M. Asiri, H. Garcia, Adv. Mater. 31 (2019) 1900617.
[47] X. Zhang, J. Han, J. Guo, Z. Tang, Small Struct. 2 (2021) 2000141.
[48] X. He, F. Yin, H. Wang, B. Chen, G. Li, Chin. J. Catal. 39 (2018) 207–227.
[49] X. Li, Z. Wang, L. Wang, Small Sci. 1 (2021) 2000074.
[50] T. Xia, Y. Lin, W. Li, M. Ju , Chin. Chem. Lett. 32 (2021) 2975–2984.

[51] Y.P. Wu, W. Zhou, J. Zhao, et al., Angew. Chem. Int. Ed. 56 (2017) 13001–13005.
[52] L. Qi, Y.Q. Su, Z. Xu, et al., J. Mater. Chem. A 8 (2020) 22974–22982.
[53] M. Zhao, W. Li, J. Li, W. Hu, C.M. Li, Adv. Sci. 7 (2020) 2001965.
[54] D. Zhu, J. Liu, Y. Zhao, Y. Zheng, S.Z. Qiao, Small 15 (2019) 1805511.
[55] M. Jahan, Z. Liu, K.P. Loh, Adv. Funct. Mater. 23 (2013) 5363–5372.
[56] H. Huang, Y. Zhao, Y. Bai, et al., Adv. Sci. 7 (2020) 2000012.
[57] Y. Sun, Z. Xue, Q. Liu, et al., Nat. Commun. 12 (2021) 1369.
[58] R. Dong, Z. Zheng, D.C. Tranca, et al., Chem. Eur. J. 23 (2017) 2255–2260.
[59] Z. Chen, H. Qing, K. Zhou, D. Sun, R. Wu, Prog. Mater. Sci. 108 (2020) 100618.
[60] M. Kuang, Q. Wang, P. Han, G. Zheng, Adv. Energy Mater. 7 (2017) 1700193.
[61] G. Anandhababu, Y. Huang, D.D. Babu, M. Wu, Y. Wang, Adv. Funct. Mater. 28 (2018) 1706120.
[62] S.M. Oh, S.B. Patil, X. Jin, S.J. Hwang, Chem. Eur. J. 24 (2018) 4757–4773.
[63] P. Karthick Kannan, P. Shankar, C. Blackman, C.H. Chung, Adv. Mater. 31 (2019) 1803432.
[64] Y. Chen, Z. Fan, Z. Zhang, et al., Chem. Rev. 118 (2018) 6409–6455.
[65] H. Liu, H. Tang, M. Fang, et al., Adv. Mater. 28 (2016) 8170–8176.
[66] R. Shen, J. Xie, Q. Xiang, et al., Chin. J. Catal. 40 (2019) 240–288.
[67] X. Zeng, Y. Zhao, X. Hu, G.D. Stucky, M. Moskovits, Small Struct. 2 (2021) 2000138.
[68] R. Gusmão, Z. Sofer, D. Bouša, M. Pumera, Angew. Chem. Int. Ed. 56 (2017) 14417–14422.
[69] C. Gibaja, M. Assebban, I. Torres, et al., J. Mater. Chem. A 7 (2019) 22475–22486.
[70] C. Li, Y. Xu, S. Liu, et al., ACS Sustain. Chem. Eng. 7 (2019) 15747–15754.
[71] J. Fan, J. Wu, X. Cui, et al., J. Am. Chem. Soc. 142 (2020) 3645–3651.
[72] A. Mahmood, H. Lin, N. Xie, X. Wang, Chem. Mat. 29 (2017) 6329–6335.
[73] S.W. Jang, S. Dutta, A. Kumar, et al., ACS Nano 14 (2020) 10578–10588.
[74] T.P. Yadav, C.F. Woellner, T. Sharifi, et al., ACS Nano 14 (2020) 7435–7443.
[75] J.Q. Chi, M. Yang, Y.M. Chai, et al., J. Energy Chem. 48 (2020) 398–423.
[76] J. Wang, H. Zhang, X. Wang, Small Method 1 (2017) 1700118.
[77] K. Hu, T. Ohto, Y. Nagata, et al., Nat. Commun. 12 (2021) 203.
[78] X. Zheng, J. Xu, K. Yan, et al., Chem. Mat. 26 (2014) 2344–2353.
[79] L. Li, D. Zhang, J. Deng, Y. Gou, J. Fang, J. Energy Chem. 49 (2020) 365–374.
[80] Y. Fujita, H.O. Venterink, P.M. Van Bodegom, et al., Nature 505 (2014) 82–86.
[81] J. Si, J. Yu, Y. Shen, M. Zeng, L. Fu, Small Struct. 2 (2021) 2000101.
[82] X. Wang, L. Bai, J. Lu, et al., Angew. Chem. Int. Ed. 58 (2019) 19060–19066.
[83] Y. Li, W. Pei, J. He, et al., ACS Catal. 9 (2019) 10870–10875.
[84] X. Li, L. Xiao, L. Zhou, et al., Angew. Chem. Int. Ed. 59 (2020) 21106–21113.
[85] R. He, J. Hua, A. Zhang, et al., Nano Lett. 17 (2017) 4311–4316.
[86] Y. Cai, J. Gao, S. Chen, et al., Chem. Mat. 31 (2019) 8948–8956.
[87] B. Zhao, Z. Wan, Y. Liu, et al., Nature 591 (2021) 385–390.
[88] C. Tan, X. Cao, X.J. Wu, et al., Chem. Rev. 117 (2017) 6225–6331.
[89] H. Tributsch, J.C. Bennett, J. Electronanal. Chem. 81 (1977) 97–111.
[90] B. Hinnemann, P.G. Moses, J. Bonde, et al., J. Am. Chem. Soc. 127 (2005) 5308–5309.
[91] J. Wei, G. Wang, Y. Zhang, et al., Chin. Chem. Lett. 32 (2021) 1191–1196.
[92] S. Hua, D. Qu, L. An, et al., Chin. J. Catal. 38 (2017) 1028–1037.
[93] K. Jiang, M. Luo, Z. Liu, et al., Nat. Commun. 12 (2021) 1687.
[94] H.I. Karunadasa, E. Montalvo, Y. Sun, et al., Science 335 (2012) 698.
[95] T.F. Jaramillo, K.P. Jørgensen, J. Bonde, et al., Science 317 (2007) 100.
[96] J. Hu, C. Zhang, Y. Zhang, et al., Small 16 (2020) 2002212.
[97] D. Voiry, M. Salehi, R. Silva, et al., Nano Lett. 13 (2013) 6222–6227.
[98] E.E. Benson, H. Zhang, S.A. Schuman, et al., J. Am. Chem. Soc. 140 (2018) 441–450.
[99] H. Wang, X. Xiao, S. Liu, et al., J. Am. Chem. Soc. 141 (2019) 18578–18584.
[100] J. Zhang, T. Wang, P. Liu, et al., Energy Environ. Sci. 9 (2016) 2789–2793.
[101] O. Lehtinen, H.P. Komsa, A. Pulkin, et al., ACS Nano 9 (2015) 3274–3283.
[102] S. Deng, F. Yang, Q. Zhang, et al., Adv. Mater. 30 (2018) 1802223.
[103] Z. Luo, J. Ge, C. Liu, W. Xing, J. Energy Chem. 41 (2020) 15–19.
[104] Z. Luo, H. Zhang, Y. Yang, et al., Nat. Commun. 11 (2020) 1116.
[105] H. Huang, J. Zha, S. Li, C. Tan , Chin. Chem. Lett. 33 (2022) 163–176.
[106] Y. Zhang, D. Yao, B. Xia, et al., Small Sci. 1 (2021) 2000052.
[107] X. Gao, B. Li, X. Sun, et al. , Chin. Chem. Lett. 32 (2021) 3591–3595.
[108] J. Azadmanjiri, P. Kumar, V.K. Srivastava, Z. Sofer, ACS Appl. Nano Mater. 3 (2020) 3116–3143.
[109] Q. Tang, D.E. Jiang, ACS Catal. 6 (2016) 4953–4961.
[110] X. Chen, Y. Qiu, G. Liu, et al., J. Mater. Chem. A 5 (2017) 11357–11363.
[111] D. Gao, B. Xia, Y. Wang, et al., Small 14 (2018) 1704150.
[112] W. Cui, Z.Y. Hu, R.R. Unocic, G. Van Tendeloo, X. Sang, Chin. Chem. Lett. 32 (2021) 339–344.
[113] L. Huang, L. Ding, H. Wang, Small Sci. (2021) 2100013.
[114] K. Li, S. Zhang, Y. Li, J. Fan, K. Lv, Chin. J. Catal. 42 (2021) 3–14.
[115] H. Pan, Sci. Rep. 6 (2016) 32531.
[116] Y. Gao, H. Zhuo, Y. Cao, et al., Chin. J. Catal. 40 (2019) 152–159.
[117] H. Lind, B. Wickman, J. Halim, et al., Adv. Sustain. Syst. 5 (2021) 2000158.
[118] J. Zhang, Y. Zhao, X. Guo, et al., Nat. Catal. 1 (2018) 985–992.
[119] Y. Jiang, T. Sun, X. Xie, et al., ChemSusChem 12 (2019) 1368–1373.
[120] A.D. Handoko, K.D. Fredrickson, B. Anasori, et al., ACS Appl. Energy Mater. 1 (2018) 173–180.
[121] W. Xiao, D. Yan, Y. Zhang, X. Yang, T. Zhang, Energy Fuels 35 (2021) 4609–4615.
[122] D. Geng, X. Zhao, Z. Chen, et al., Adv. Mater. 29 (2017) 1700072.
[123] Y. Liu, H. Xiao, W.A. Goddard, J. Am. Chem. Soc. 138 (2016) 15853–15856.
[124] C. Cui, R. Cheng, C. Zhang, X. Wang, Chin. Chem. Lett. 31 (2020) 988–991.
[125] A. Han, Z. Zhang, X. Li, et al., Small Method 4 (2020) 2000248.
[126] P.M. Bodhankar, P.B. Sarawade, G. Singh, A. Vinu, D.S. Dhawale, J. Mater. Chem. A 9 (2021) 3180–3208.
[127] J. Yu, Q. Wang, D. O'Hare, L. Sun, Chem. Soc. Rev. 46 (2017) 5950–5974.
[128] Z. Cao, B. Li, L. Sun, et al., Small Method 4 (2020) 1900343.
[129] Y. Zhai, X. Ren, J. Yan, et al., Small Struct. 2 (2021) 2000096.
[130] H. Yang, Z. Chen, P. Guo, B. Fei, R. Wu, Appl. Catal. B: Environ. 261 (2020) 118240.
[131] H. Yin, S. Zhao, K. Zhao, et al., Nat. Commun. 6 (2015) 6430.
[132] C. Xia, Y. Zhou, C. He, et al. , Small Sci. 1 (2021) 2100010.
[133] L. Huang, S. Zaman, Z. Wang, et al., Acta Phys. Chim. Sin. 37 (2021) 2009035.
[134] Y. Yang, M. Wu, X. Zhu, et al., Chin. Chem. Lett. 30 (2019) 2065–2088.